Extended Abstracts of the 2009 International Conference on Solid State Devices and Materials, Sendai, 2009, pp1100-1101

Shell Strain Effects on Valence Band Structure and Transport Property in $Ge/Si_{1-x}Ge_x$ Core-Shell Nanowire

Honghua Xu[1], Yuning Zhao[1], Yuhui He[1], Chun Fan[2], *Gang Du[1], *Xiaoyan Liu[1], Ruqi Han[1] and Jinfeng Kang[1]

[1]Institute of Microelectronics, Peking University & Key Laboratory of Microelectronic Devices and Circuits, Ministry of education, Beijing 100871, China *Email: gang_du@ime.pku.edu.cn; xyliu@ime.pku.edu.cn

[2]Computer Center of Peking University, Beijing 100871, China

Introduction

To date, Ge NW based devices are of renewed interest owing to higher bulk mobility with good process compatibility. [1-3]An active area has been improving those NW devices. The realization of core-shell structures with lattice misfit strain offers intriguing chances for improving NW performance. The introduction of strain effects near interfaces can tailor valence band structures. [4] And the optimization of shell materials or compositions during NW heteroepitaxy process is possible to modulate the device property. [2] $Si_{1-x}Ge_x$ as a shell based NW device is demonstrated a high performance recently. [5] However, there is a paucity of theoretical study on the strained device performance with a $Si_{1-x}Ge_x$ shell in core-shell NWs.

In this work, we calculate the varied strain induced by thickness or Ge contents in shell via finite element method. Then, the strained valence band structure is computed by full 6×6 Luttinger-Kohn Hamiltonian. [6-7] The hole mobility is calculated using modified Kubo-Greenwood formula. [8] The results can help to be a guideline to design NW FETs with core-shell structures.

Simulation Methodology

Based on continuum elastic model, [9] the $Si_{1-x}Ge_x$ shell strain energy expression is as follows:

$$\begin{aligned} U_s = \frac{1}{2}\iint_S ds\{ & D_1' \ [(\varepsilon_{xx}-\varepsilon_{xx}^S)^2+(\varepsilon_{yy}-\varepsilon_{yy}^S)^2] \\ & + D_2' \ (\frac{a_z}{a_z^0}-1-\varepsilon_{zz}^S)+D_3' \ (\varepsilon_{xx}-\varepsilon_{xx}^S)(\varepsilon_{yy}-\varepsilon_{yy}^S) \\ & + D_4' \ [(\varepsilon_{xx}-\varepsilon_{xx}^S)+(\varepsilon_{yy}-\varepsilon_{yy}^S)](\frac{a_z}{a_z^0}-1-\varepsilon_{zz}^S) \\ & + D_5' \ (\varepsilon_{xy}-\varepsilon_{xy}^S)^2\} \end{aligned} \tag{1}$$

$$\begin{aligned} & D_1' = D_2' = \frac{E_s(1-\nu)}{(1+\nu)(1-2\nu)}; D_3' = D_4' = \frac{2E_s\nu}{(1+\nu)(1-2\nu)}; \\ & D_5' = \frac{E_s}{(1+\nu)}; \varepsilon_{ii}^S = \frac{a_i^s}{a_z^0}-1; \end{aligned} \tag{2}$$

The core strain energy has a similar form through coordinate transformation. [9]The shell lattice constant is related to the thickness difference, the shear modulus variation and the lattice misfit factor between core and shell layers. [10] E_s is the Young modulus and v is Poisson ratio of $Si_{1-x}Ge_x$ shell. [11] And x is the Ge contents in shell. $\varepsilon_{ij}(\varepsilon^S_{ij})$ are strain tensor components in Ge core (shell). All NWs' radii in core are fixed 5nm here. The strained valence band structures are calculated via a generalized ***k·p*** method and Bessel basis function. [6] Hole density and potential distribution are calculated by self-consistently solving Poisson and density distribution equations. The hole mobility limited by acoustic-phonon and optical-phonon scatterings are also evaluated. [8]

Results and Discussion

Fig.1 shows strain energy distribution and strain tensor components in Ge (110) NW with 2nm thick $Si_{0.8}Ge_{0.2}$ shell. Fig.2 (a) shows valence band structure in pure Ge (110) NW. Compared to NW with 1nm (b) and 2nm (c) thick $Si_{0.8}Ge_{0.2}$, strained valence subbands remarkably shift upwards and warps as the shell increases. Fig.3 shows valence band structures in NW with various Ge contents in shell. As the Ge contents reduces from x=0.6 (a) to x=0.4 (b), the valence subbands go up. When the shell is the Si (110) crystal in Fig.3(c), the shifting and warping degree of the subbands is more obvious. Effective masses of top five subbands versus shell thickness and Ge concentration in shell are shown in Fig.4. As the shell becomes thicker, effective masses turn into lower values. But as the Ge contents increases, most effective masses moves larger. Fig.5 plots hole density distribution in Ge NW with 2nm $Si_{0.6}Ge_{0.4}$ at 0V, -1V gate voltage. As V_G increases to -1V, the peak hole density in the core increases from 10^{18} cm^{-3} to 10^{20} cm^{-3}. Fig.6 shows the potential distribution in Ge NW with 2nm $Si_{0.6}Ge_{0.4}$ at 0V, -1V gate voltage in a cross section. Fig.7 plots the hole mobility versus effective electric field with 0, 1nm, 2nm thick $Si_{0.8}Ge_{0.2}$ shell. The hole mobility is larger with thicker shell. This is caused by larger lattice-misfit strain effects. Fig.8 illustrates the hole mobility versus effective electric field with various Ge contents in shell. The hole mobility increases as the Ge content in shell reduces. NW with Si (110) shell has the largest hole mobility.

Conclusions

Strain induced valence band and hole transport in $Ge/Si_{1-x}Ge_x$ hetero-structure nanowires are investigated. The valence subbands shift upwards and warp as the shell thickness increases or the Ge concentration in shell reduces. The hole mobility with phonon-limited scattering also increases with the thicker shell or lower Ge contents in shell. Our calculation results are useful to optimize the core-shell hetero-structure nanowire performance.

Acknowledgement

This work is supported by 107003, NKBRP2006 CB302705.

References

[1] A.B.Greytak, L.J.Lauhon, M.S.Gudiksen, et al. Appl. Phys. Lett 84 (2004) 4176. [2] J.Xiang, W.Lu, Y.J.Hu, et al. Nature 441 (2006) 489. [3]T.I.Kamins, X.Li, R.S.Williams, et al. Nano.Lett 4(3) (2004) 503. [4] Y. He, Y. Zhao, S. Yu,et al. IEDM (2008) 189. [5] J.Nah, E.S.Liu, D.Shanhrjerdi,et al. Appl.Phys.Lett 94 (2009) 063117. [6] J.M.Luttinger, W.Kohn. Phys.Rev 97 (1955) 869. [7] C.Y.P.Chao, S.L.Chuang. Phys.Rev.B 46 (1992) 4110. [8]R.Kotlyar, B.Obradovic, P.Matagne, et al. Appl.Phys.Lett 84 (2004) 5270. [9] Y. He, C.Fan,Y. Zhao,et al. SISPAD (2008) 121. [10]D.J.Paul.Semi.Sci.Tech 19 (2004) 75. [11]J.J.Wortman and R.A.Evans. J.Appl.Phys 36 (1965) 153.

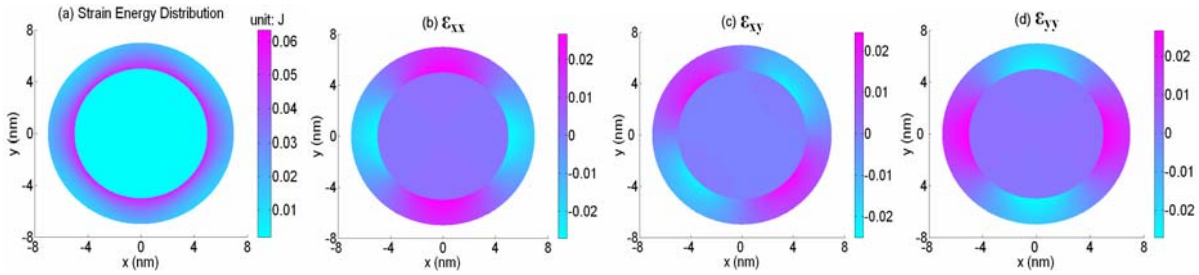

Fig. 1 Strain energy distribution (a) and strain tensor components ε_{xx} (b), ε_{xy} (c), ε_{yy} (d) in Ge (110) NW with 2nm thick $Si_{0.8}Ge_{0.2}$ shell (R=5nm)

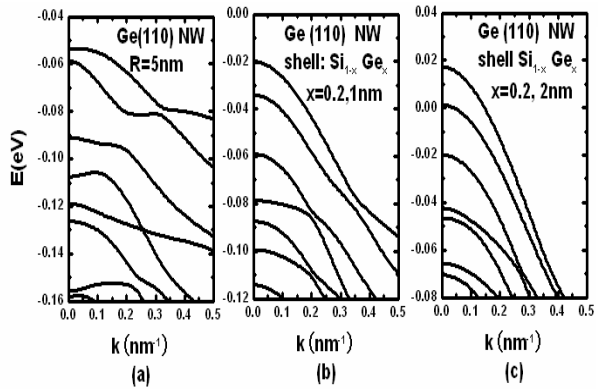

Fig.2 Valence band structures in pure Ge (110) NW (a), with $Si_{0.8}Ge_{0.2}$ shell: 1nm (b) and 2nm (c)

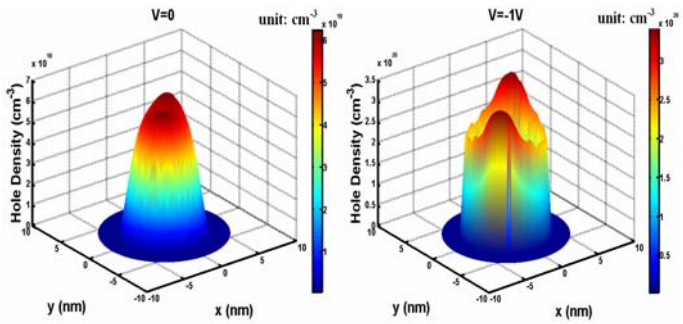

Fig.5 Hole density distribution ρ(r) in Ge (110) NW with 2nm thick $Si_{0.6}Ge_{0.4}$ shell at V_G=0 (left), V_G=-1V (right)

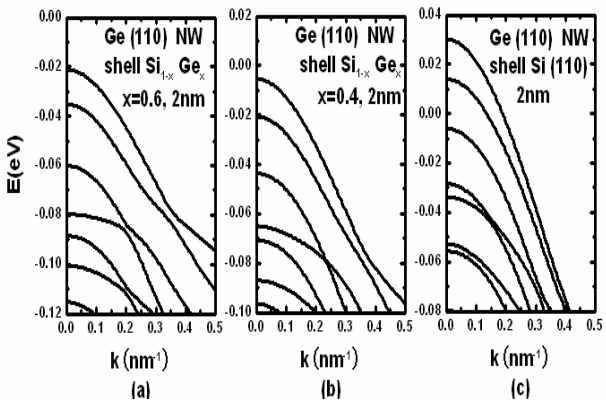

Fig. 3 Valence band structures in Ge (110) NW with $Si_{0.4}Ge_{0.6}$ shell (a), $Si_{0.6}Ge_{0.4}$ shell (b) and Si (110) crystal shell (c)

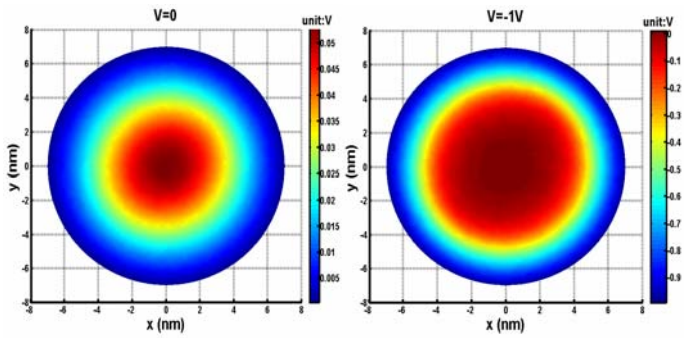

Fig. 6 Cross section of the potential distribution in Ge (110) NW with 2nm thick $Si_{0.6}Ge_{0.4}$ shell at V_G=0 (left), V_G=-1V (right), respectively

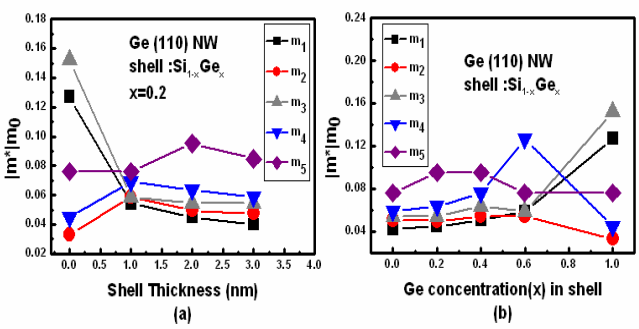

Fig. 4 Effective masses of top 5 subbands in Ge (110) NW versus shell thickness (a), and Ge concentration in shell (b)

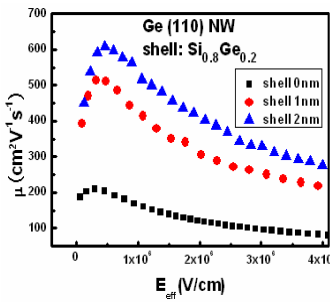

Fig. 7 Hole mobility μ versus effective electric field E_{eff} with different thickness $Si_{0.8}Ge_{0.2}$ shell

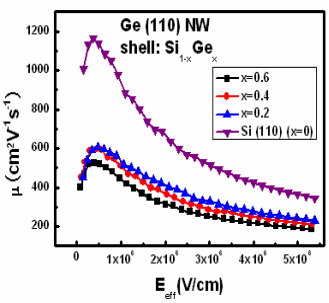

Fig. 8 Hole mobility μ versus effective electric field E_{eff} with different Ge contents in 2nm $Si_{1-x}Ge_x$ shell